# Shear-induced angular dependence of the liquid pair correlation function

H. J. M. Hanley and J. C. Rainwater
*Thermophysics Division, National Engineering Laboratory, National Bureau of Standards, Boulder, Colorado 80303*

S. Hess
*Institut für Theoretische Physik, Technische Universität Berlin (PN 7-1), D-1000 Berlin 12, West Germany*
(Received 20 March 1987)

A formal expansion in spherical harmonics or Cartesian tensors of the pair correlation function of a liquid subjected to a shear rate is discussed. Expressions for the coefficients to tensor rank 4 are evaluated via a nonequilibrium molecular-dynamics simulation of an inverse twelve soft-sphere liquid undergoing Couette flow. It is shown that the expansion converges slowly if the product $\tau\gamma > 0.05$, where $\tau$ is the Maxwell relaxation time and $\gamma$ is the shear rate. Further, the fourth-rank coefficient that represents cubic symmetry is significant for our model system. The microstructure of a shear liquid is demonstrated by intensity plots of particles around a given central particle. We have derived expressions for the expansion coefficients using a relaxation-time model and the comparison between them and the simulations is generally very good.

## I. INTRODUCTION

In nonequilibrium molecular dynamics (NEMD) one simulates the behavior of a model liquid that is perturbed away from equilibrium.[1] The technique is powerful; interpreting and debating the results has led to a reexamination of the fundamentals of nonequilibrium statistical mechanics and nonequilibrium thermodynamics.[2] The connection between simulations and real experiments is also a point of interest because the simulations indicate that the simplest model liquid under shear can display nonlinear, non-Newtonian characteristics often associated only with the rheological behavior of complex molecules. Further, one can evaluate *a priori* the coefficients that describe non-Newtonian phenomena for a model system. Thus non-Newtonian phenomena can be examined from a fresh viewpoint: Rather than discuss the phenomena in macroscopic terms and then infer the properties of the liquid (the traditional approach), the properties are in principle known so the macroscopic behavior can be predicted. We have done this. Given the shear-rate-dependent properties of model liquids, in particular the Lennard-Jones and the soft-sphere fluid, we have discussed light scattering from colloidal suspensions,[3] the Weissenberg effect in a stirred liquid (rod climbing phenomenon),[4] the flow behavior of a coal slurry,[5] and shear-induced phase transitions in mixtures.[6]

A key to understanding such phenomena in a sheared fluid is to understand the behavior of the pair correlation function $g(\mathbf{r},\gamma)$ or the structure factor $S(\mathbf{k},\gamma)$. Here $\mathbf{r}$ is the vector separation between a reference particle and another particle, $\mathbf{k}$ is the wave vector, and $\gamma$ is the shear rate. The variation of $g(\mathbf{r},\gamma)$ with shear rate gives a quantitative picture of the distortion and relaxation of the fluid structure, and appropriate integration gives the fluid's properties. The object of this paper is to discuss the evaluation of the correlation function, specifically to expand $g(\mathbf{r},\gamma)$ in spherical harmonics,[7,8] or in the equivalent Cartesian tensors[9] constructed from the components of $\hat{\mathbf{r}}=\mathbf{r}/r$, and to estimate the expansion coefficients by simulation. Finally we will show how the coefficients can be predicted via a relaxation-time model.[10]

We have looked at this problem in our previous work[10,11] when an expansion for the pair correlation function to tensor rank 2 was derived. Recent computer simulations show, however, that the anisotropy of a sheared system can be substantial when the shear rate is high,[12,13] and a truncated series to rank 2 is too simple. Accordingly, the series is extended to rank 4 in this paper. In so doing we thought it worthwhile to present the series expansion in a more systematic manner than before.

The article is organized as follows. The expansion for $g(\mathbf{r},\gamma)$ is derived. The expansion coefficients for a system of 864 particles interacting with the $1/r^{12}$ soft-sphere potential are estimated. The coefficients are then used to construct intensity plots for $g(\mathbf{r},\gamma)$. Finally, we extend the relaxation-time model of Ref. 10 to coefficients of rank 4, and compare these theoretical results with the simulations.

## II. EXPANSION OF THE PAIR CORRELATION FUNCTION

### A. Spherical harmonics and Cartesian tensors

The pair correlation function can be expressed in terms of spherical harmonics $Y_{lm}^{*}(\hat{\mathbf{r}})$ as

$$g(\mathbf{r})=g_s(r)+\sum_{l=1}^{\infty}\sum_{m=-l}^{l} g_{lm}(r)Y_{lm}^{*}(\hat{\mathbf{r}}) , \tag{1}$$

where we have written $g(\mathbf{r},\gamma)$, etc., as $g(\mathbf{r})$ for convenience. The scalar contribution is

$$g_s(r)=\frac{1}{4\pi}\int g(\mathbf{r})d\hat{\mathbf{r}} \tag{2}$$

and the expansion coefficients are

$$g_{lm}(r)=\int Y_{lm}(\hat{\mathbf{r}})g(\mathbf{r})d\hat{\mathbf{r}} , \tag{3}$$

when $d\hat{\mathbf{r}}$ is the solid angle element on the unit sphere surrounding a central reference particle.

An alternative expansion for $g(\mathbf{r})$ is, via Cartesian tensors[13,14]

$$g(\mathbf{r})=g_s(r)+\sum_l g^{(l)}_{\mu_1\mu_2\cdots\mu_l}(r)\phi_{\mu_1\mu_2\cdots\mu_l}(\hat{\mathbf{r}}) , \tag{4}$$

with

$$\phi_{\mu_1\mu_2\cdots\mu_l}(\hat{\mathbf{r}})=\xi_l r^{-l}\overline{r_{\mu_1}r_{\mu_2}\cdots r_{\mu_l}} , \tag{5}$$

where the overbar indicates the symmetric traceless part of a tensor and for the special case of rank 2,

$$\overline{a_\mu b_\nu}\equiv\tfrac{1}{2}(a_\mu b_\nu+a_\nu b_\mu)-\tfrac{1}{3}a_\lambda b_\lambda\delta_{\mu\nu} , \tag{6}$$

with $\delta_{\mu\nu}$ the unit tensor. The Cartesian components are denoted by Greek subscripts and the summation convention applies. Note that the $g_s(r)$ of Eq. (4) is shear dependent and is not the radial distribution function $g_{\rm eq}(r)$ of the fluid at rest.

For general $l$, a traceless symmetric tensor is by definition symmetric under interchange of any pair of indexes and vanishes after contraction of any pair of indexes. For example, the $\phi$ tensor for $l=4$ is given by Eq. (1.6) of Ref. 9. Cartesian tensors have the property that

$$\mathbf{A}_{\mu_1\mu_2\cdots\mu_l}\overline{\mathbf{B}}_{\mu_1\mu_2\cdots\mu_l}=\overline{\mathbf{A}}_{\mu_1\mu_2\cdots\mu_l}\overline{\mathbf{B}}_{\mu_1\mu_2\cdots\mu_l} . \tag{7}$$

Thus Eq. (4) does not uniquely define $g^{(l)}_{\mu_1\mu_2\cdots\mu_l}(r)$, since two different tensors with the same traceless symmetric part yield the same result. However, the expansion can be made unique by requiring that $g^{(l)}_{\mu_1\mu_2\cdots\mu_l}(r)$ be traceless symmetric.

The normalization coefficients are given by

$$\xi_l=[(2l+1)!!/l!]^{1/2} \tag{8}$$

and the expansion coefficients are obtained from inversion of Eq. (4),

$$g^{(l)}_{\mu_1\mu_2\cdots\mu_l}(r)=\frac{1}{4\pi}\int\phi_{\mu_1\mu_2\cdots\mu_l}(\hat{\mathbf{r}})g(\mathbf{r})d\hat{\mathbf{r}} . \tag{9}$$

### B. Plane Couette geometry

For pure simple fluids $g(\mathbf{r})=g(-\mathbf{r})$, so only even values of $l\geq 2$ occur in the summations of Eqs. (1) and (4) and there will be $(2l+1)$ expansion coefficients for each $l$ in general. Moreover, we can choose special symmetries that will further simplify the expansions. In fact it is most convenient to consider a fluid subjected to plane Couette flow. Define a fluid with velocity $\mathbf{v}$ subjected to a shear rate $\gamma$ so

$$\gamma=\partial v_x/\partial y=\text{const} , \tag{10}$$

hence

$$v_x=\gamma y, \quad v_y=v_z=0 . \tag{11}$$

In this case the only expansion coefficients of Eqs. (1) or (4) are those associated with the exchange $(x,y,z)\rightarrow(-x,-y,z)$, i.e., only $(l+1)$ of $(2l+1)$ terms occur.

Equations (10) and (11) are a special case of the more general linear flow profile, where $\mathbf{e}^x$ and $\mathbf{e}^y$ are unit basis vectors,

$$\mathbf{v}=\gamma y\mathbf{e}^x+\alpha\gamma x\mathbf{e}^y \tag{12}$$

which also obeys the above "Couette symmetry." Plane Couette flow corresponds to $\alpha=0$, rigid rotation to $\alpha=-1$, and "four-roller flow" to $\alpha=+1$.

An objective of the paper is to expand the pair correlation function to rank 4. For plane Couette flow, the most general form for the tensors of Eq. (9) is given in Eqs. (A1) and (A2) of the Appendix. Upon substituting these forms into Eq. (4) and performing the contractions, made simpler with Eq. (7), we obtain

$$\begin{aligned} g(\mathbf{r})&=g_s(r)+\sum_l\sum_k g^{(l)}_k X^{(l)}_k(\hat{\mathbf{r}}) \\ &=g_s(r)+g^{(2)}_0X^{(2)}_0+g^{(2)}_1X^{(2)}_1+g^{(2)}_2X^{(2)}_2 \\ &\quad+g^{(4)}_0X^{(4)}_0+g^{(4)}_1X^{(4)}_1\cdots g^{(4)}_4X^{(4)}_4+\cdots , \end{aligned} \tag{13}$$

where if $\hat{x}$, $\hat{y}$, and $\hat{z}$ are the components of $\hat{\mathbf{r}}$ we have for rank 2,[15]

$$\begin{aligned} X^{(2)}_0&=\hat{z}^2-\tfrac{1}{3} , \\ X^{(2)}_1&=\tfrac{1}{2}(\hat{x}^2-\hat{y}^2) , \\ X^{(2)}_2&=\hat{x}\hat{y} , \end{aligned} \tag{14}$$

and for rank 4,

$$\begin{aligned} X^{(4)}_0&=\hat{z}^4-\tfrac{6}{7}\hat{z}^2+\tfrac{3}{35} , \\ X^{(4)}_1&=\tfrac{1}{2}(\hat{x}^2-\hat{y}^2)(\hat{z}^2-\tfrac{1}{7}) , \\ X^{(4)}_2&=\hat{x}\hat{y}(\hat{z}^2-\tfrac{1}{7}) , \\ X^{(4)}_3&=\tfrac{1}{4}(\hat{x}^4+\hat{y}^4-6\hat{x}^2\hat{y}^2) , \\ X^{(4)}_4&=\hat{x}\hat{y}(\hat{x}^2-\hat{y}^2) . \end{aligned} \tag{15}$$

The expansion coefficients are [cf. Eq. (9)]

$$g^{(l)}_k(r)=\xi_l^2C^{(l)}_k\left[\frac{1}{4\pi}\right]\int X^{(l)}_k(\hat{\mathbf{r}})g(\mathbf{r})d\hat{\mathbf{r}} , \tag{16}$$

where $C^{(l)}_k$ is a coefficient with the values for $l=2$ and 4,

$$\begin{aligned} &C^{(2)}_0=\tfrac{3}{2}, \quad C^{(2)}_1=C^{(2)}_2=2 , \\ &C^{(4)}_0=\tfrac{35}{8}, \quad C^{(4)}_1=C^{(4)}_2=14 , \\ &C^{(4)}_3=C^{(4)}_4=2 . \end{aligned} \tag{17}$$

The $X^{(l)}_k$ functions are closely related to the spherical harmonics. For even nonzero $k$, $X^{(l)}_k$ is proportional to $\mathrm{Im}Y_{lm}$, $m=k$; for odd $k$, $X^{(l)}_k$ is proportional to $\mathrm{Re}Y_{lm}$, $m=k+1$; for zero $k$, $X^{(l)}_k$ is proportional to $Y_{l0}$.

## III. COMPUTER SIMULATION

We used the same computer procedure here as reported in our previous work,[10,11] namely, we simulated Couette

flow of a soft-sphere liquid with the potential $\phi = 1/r^{12}$ at the state point $\rho(4T)^{-1/4}$ with the temperature[16] $T$ set at $\frac{1}{4}$: $\rho$ is the density, $\rho = N/V$ with $N$ the number of particles in volume $V$. Runs were carried out at $\rho = 0.8$ and $\rho = 0.7$ with $N = 108$, 256, 500, and 864 for the system in equilibrium and when subjected to several values of the imposed shear in the range $0.01 \leq \gamma \leq 2.0$. The algorithm was a very minor variant of that described by Evans and Morriss[1] and makes use of the Gaussian equations of motion, i.e., $\ddot{\mathbf{r}}_i = (1/m)\mathbf{F}_i - \lambda \dot{\mathbf{r}}_i$ where $\mathbf{F}_i$ is the force on particle $i$ and $\lambda$ is a multiplier given by $\lambda = \sum \dot{\mathbf{r}}_j \cdot \mathbf{F}_j / (m \sum \dot{r}_j^2)$. The power of this algorithm is that the kinetic temperature is a constant of the equation of motion so one can work in the convenient $(N, V, T)$ ensemble.

Estimates of the functions $g_k^{(l)}(r)$ follow directly by constructing histograms of the appropriate moments of $r$ as given by Eqs. (14) and (15); see, for example, Ref. 11.

We first worked with the system at $\rho = 0.8$ and $\gamma = 2.0$ for $N = 108$, so chosen because we knew the signal-to-noise ratio for the histograms was strong in this case. We observed that the $g_3^{(4)}$ coefficient was large and dominated the $g_k^{(4)}$ series. To check the effect of system size, runs were repeated for $N = 256$, 500, and 864 particles but we found that $N$ had only a small influence on the values of all $g_k^{(4)}$, and that $g_3^{(4)}$ was indeed the most significant. Subsequent simulations were made for a 864-particle system at $\rho = 0.7$ for 5000–10 000 time steps with $\Delta t = 0.003$. The change in density was advisable because it is now realized that $\rho = 0.8$ is too close to the freezing transition and its associated complications, discussed elsewhere.[12,13]

Sample results are shown in Figs. 1 and 2 for $\gamma = 1.0$. The plots for $g_k^{(2)}$ are equivalent to similar plots published previously.[10] The curves for $g_k^{(4)}$ are new. The general pattern of Figs. 1 and 2 was obtained for all values of $\gamma$, only that the $g_k^{(4)}$ are small for $\gamma < 0.5$ with $g_3^{(4)}$ the most prominent.

It is interesting to represent the expansion coefficients through an intensity plot[17] of $g(\mathbf{r})$, i.e., the intensity with respect to the average of particles around a given central particle. For example, let us write the expansion of Eq. (13) in polar coordinates for the shear plane: $\hat{x} = \cos\phi$, $\hat{y} = \sin\phi$, and $\hat{z} = 0$. We have, through rank 4,

$$g(\mathbf{r}) = g_s - \tfrac{1}{3} g_0^{(2)} + \tfrac{3}{35} g_0^{(4)} + (\tfrac{1}{2} g_1^{(2)} - \tfrac{1}{14} g_1^{(4)}) \cos(2\phi) + (\tfrac{1}{2} g_2^{(2)} - \tfrac{1}{14} g_2^{(4)}) \sin(2\phi) + \tfrac{1}{4} g_3^{(4)} \cos(4\phi) + \tfrac{1}{4} g_4^{(4)} \sin(4\phi) \, . \quad (18)$$

Since we have $g_k^{(l)}$ as a function of $r$, we can construct graphs such as Figs. 3–5 for our system at $\rho = 0.7$ and $\gamma = 1$. Figure 3 is essentially the intensity plot for the fluid at rest; that is, all $g_k^{(l)}$ are zero. Note that $g_s(r) \neq g_{\text{eq}}(r)$ as remarked, however. The graph is radially symmetric and the highest intensity (darkest shading) corresponds to the peak in $g_s(r)$. The circle in the center is an artifact to represent the central particle. In Fig. 4 we add to $g_s(r)$ the three $g_k^{(2)}$ terms. The pattern shifts from circular to elliptical. If only the $g_2^{(2)}$ term were added, the major axis of the ellipse would be along $\phi = \pi/4$. The effect of $g_1^{(2)}$ is to shift the axis very slightly away from $\pi/4$. For $\rho = 0.7$ and $\gamma = 1$, the changes due to $g_1^{(2)}$ and $g_0^{(2)}$ are quite small, in contrast to the large and dramatic effects for $\rho = 0.8$ and $\gamma = 2$ as reported earlier for the radial distribution function[17] and the static structure factor.[3]

Figure 5 includes the $g_k^{(4)}$ terms that give rise to a further intensity variation in the second ring. It is clear that for the system at $\rho = 0.7$ and $\gamma = 1$ the $g_k^{(4)}$ terms are significant in the expansion of Eq. (13), but we can make a more general conclusion. A relaxation time $\tau$ can be defined as $\tau = \eta/G$ where $G$ is the shear modulus and $\eta$ is the shear viscosity; $\tau \approx 0.2$ for $\rho = 0.7$. If the dimensionless expansion parameter, i.e., the product $\tau\gamma$, is approximately 0.05 or less, we surmise that the expansion (13) converges rapidly and contributions with $l \geq 6$ are negligible. For the example we have illustrated, $\tau\gamma \approx 0.2$ and we conjecture that the convergent limit of $g(\mathbf{r})$ has substantially been reached, although the $l = 6$ terms might effect some subtle changes in the shapes of the primary rings.

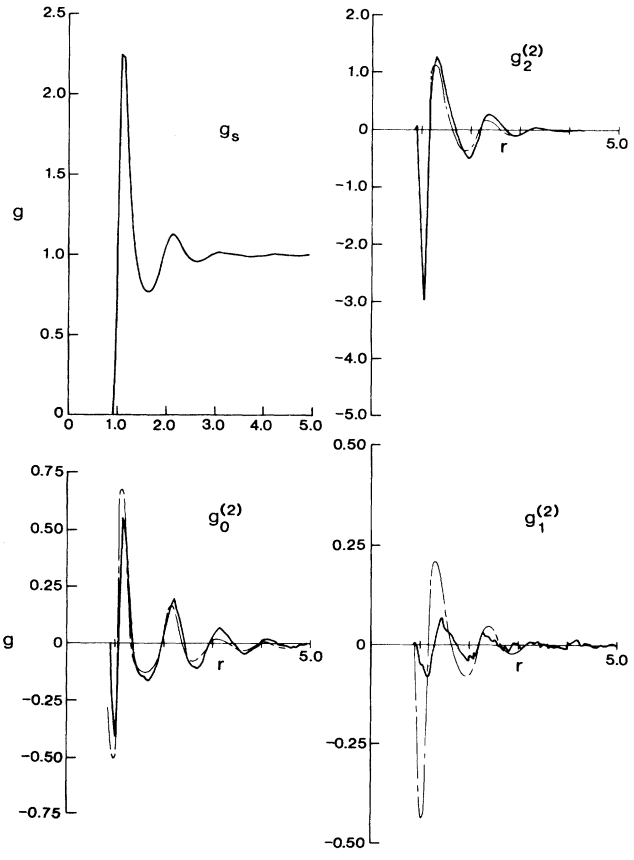


FIG. 1. Plots of the first four coefficients of Eq. (13); $g_s$ and $g_k^{(2)}$, for the soft-sphere system at $\rho = 0.7$ and $\gamma = 1.0$. The solid curves are the simulated data; the dashed curves are predicted from the Stokes-Maxwell relations of Sec. IV B. The relaxation time $\tau$ [e.g., Eq. (34)] was approximated by fitting the coefficient $g_2^{(2)}$ at the first minimum, with the result $\tau = 0.169$. Compare with the curves of Ref. 10.

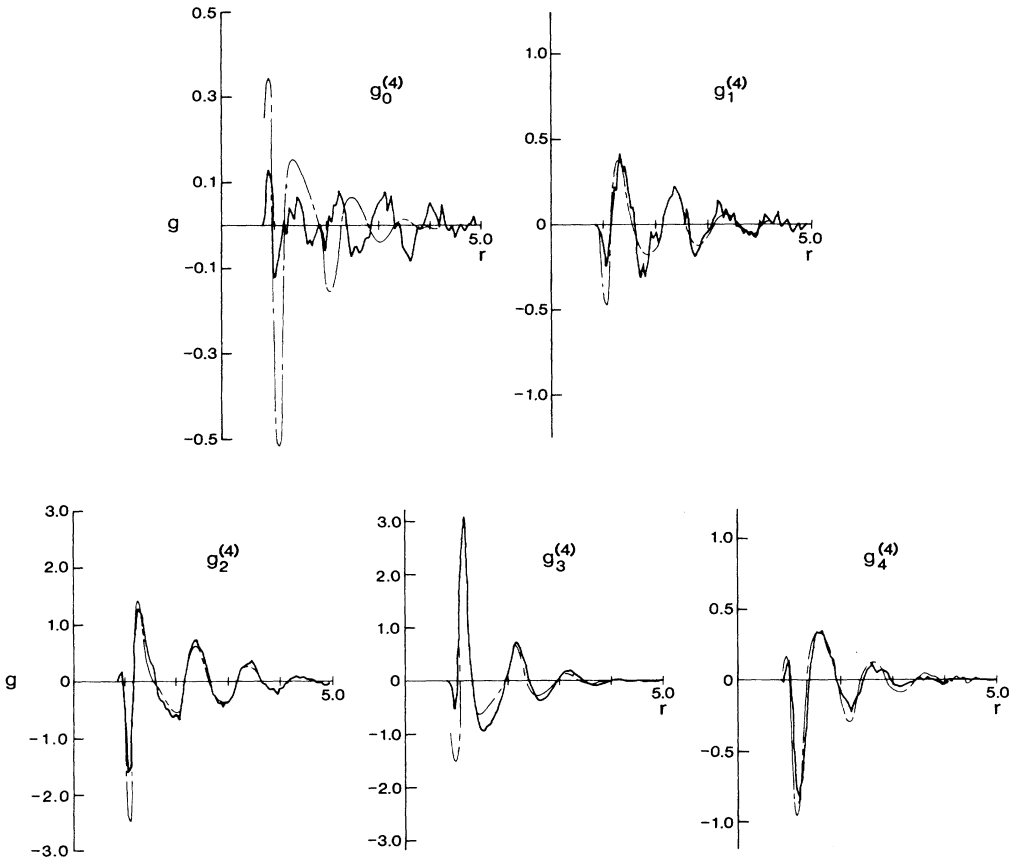


FIG. 2. Plots of the $g_k^{(4)}$ coefficients of Eq. (13). The dashed curves are predicted from the Stokes-Maxwell relations; see the caption to Fig. 1.

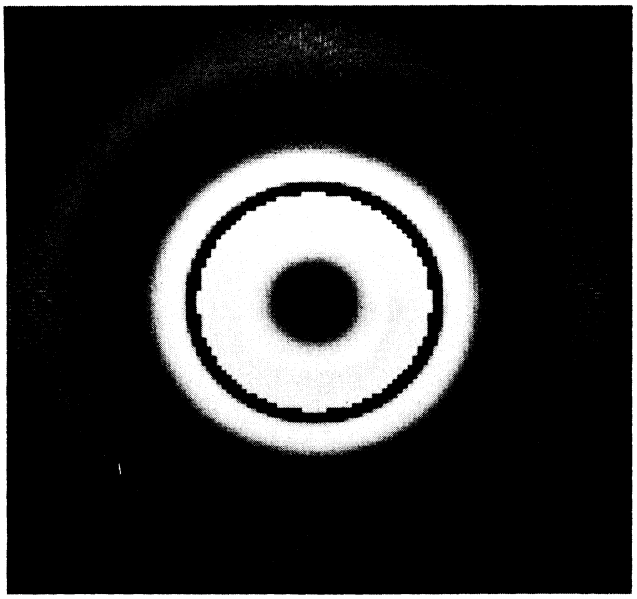

FIG. 3. Intensity plot of the scalar contribution to the distribution of particles around a central particle for the soft-sphere system at $\rho=0.7$, $\gamma=1$. The inner (darkest) ring of maximum intensity corresponds to the peak in $g_s(r)$. The center dark spot is an artifact to depict the central particle.

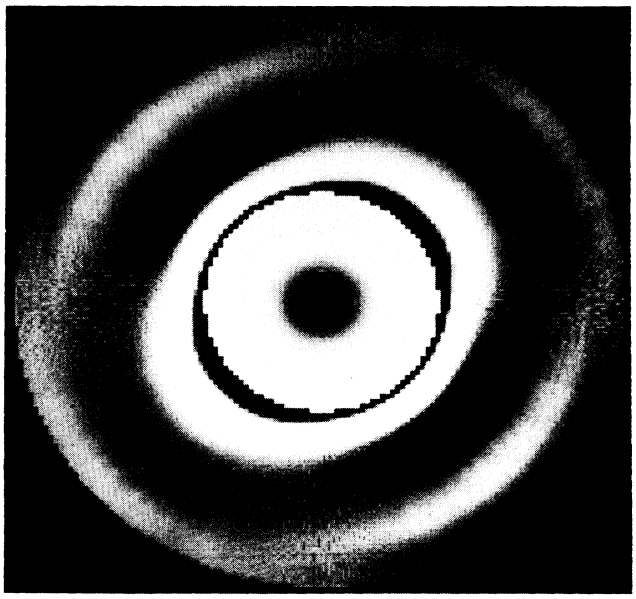

FIG. 4. Intensity plot for the soft-sphere system subjected to a shear with $\gamma=1.0$. The plot is for the plane of the shear, see Eq. (18), with all $g_k^{(2)}$ included. The major axis of the ellipse is slightly away from $\pi/4$ and there is some weak structure in the second ring.

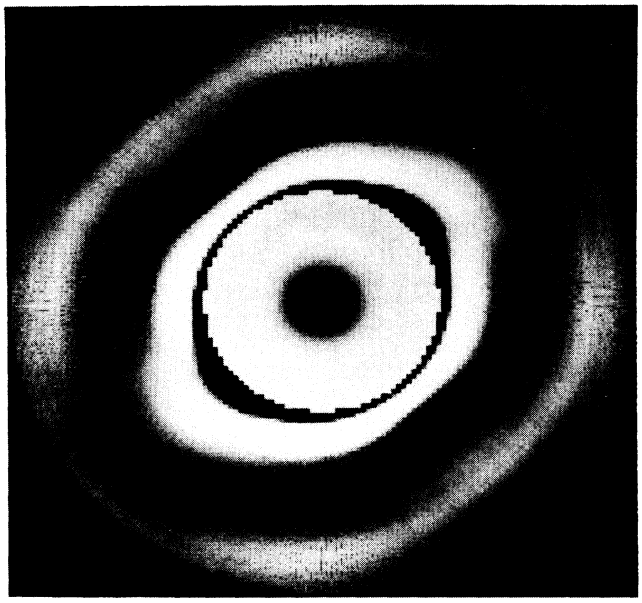

FIG. 5. In this plot all expansion coefficients of Eq. (18) are included. Note the structure changes in the second ring.

## IV. GENERALIZED STOKES-MAXWELL RELATIONS

We next develop a predictive method for the expansion coefficients. In Ref. 10 it was shown that a relaxation-time method led to expressions for $g_k^{(2)}$ in terms of the scalar coefficient $g_s$ and the time $\tau$; the simplest is well known, i.e., $g_2^{(2)}=-\tau\gamma r\, dg_s/dr$. We want to extend that approach here.

### A. Kinetic equation

The pair correlation function is assumed to obey a kinetic equation of the form[18–20]

$$\left[\left[\frac{\partial}{\partial t}\right]+(\nabla_\mu v_\nu)r_\mu\left[\frac{\partial}{\partial r_\nu}\right]+\mathcal{D}\right]g(\mathbf{r})=0\ , \tag{19}$$

which we write as

$$\left[\frac{\partial}{\partial t}+\omega_\mu\mathcal{L}_\mu+\gamma_{\mu\nu}\mathcal{L}_{\mu\nu}+\mathcal{D}\right]g(\mathbf{r})=0 \tag{20}$$

after decomposing the velocity gradient tensor into its symmetric traceless and antisymmetric parts. For the most general flow, a term $(\nabla\cdot\mathbf{v})(\mathbf{r}\cdot\partial/\partial\mathbf{r})$ would also appear within the parentheses of Eq. (20), but for Couette flow and all incompressible fluid flow $\nabla\cdot\mathbf{v}=0$. Here $\boldsymbol{\omega}$ is the vorticity

$$\boldsymbol{\omega}=\tfrac{1}{2}(\nabla\times\mathbf{v}) \tag{21}$$

and $\gamma$ is the shear rate defined formally as

$$\gamma_{\mu\nu}=\overline{\nabla_\mu v_\nu}\ . \tag{22}$$

The terms $\mathcal{L}$ are operators

$$\mathcal{L}_\mu=\left[\mathbf{r}\times\frac{\partial}{\partial\mathbf{r}}\right]_\mu,\quad \mathcal{L}_{\mu\nu}=\overline{r_\mu\frac{\partial}{\partial r_\nu}} \tag{23}$$

and $\mathcal{D}$ is a damping term that has the property

$$\mathcal{D}g_{\rm eq}(r)=0\ , \tag{24}$$

which is a consequence of the constraint that $g(\mathbf{r})$ relaxes to its equilibrium value in the absence of a viscous flow.

Let us write Eq. (4) as

$$g(\mathbf{r})=g_s(r)+g_{ns}(\mathbf{r}) \tag{25}$$

and make the specific relaxation time approximation[21] that

$$\begin{aligned}&\mathcal{D}g_s(r)=\tau_0^{-1}[g_s(r)-g_{\rm eq}(r)]\ ,\\ &\mathcal{D}g_{ns}(\mathbf{r})=\sum_{l\neq0}\tau_l^{-1}g^{(l)}_{\mu_1\mu_2\cdots\mu_l}(r)\phi_{\mu_1\mu_2\cdots\mu_l}(\hat{\mathbf{r}})\ .\end{aligned} \tag{26}$$

From this point, for simplicity we suppress the $r$ dependence of the $g$ functions. Inserting Eqs. (25) and (26) into Eq. (20), and noting that $\omega\cdot\mathcal{L}g_s=0$ leads to two coupled equations:

$$\frac{\partial}{\partial t}g_s+\frac{1}{4\pi}\int\gamma_{\mu\nu}\mathcal{L}_{\mu\nu}g_{ns}\,d\hat{\mathbf{r}}+\tau_0^{-1}(g_s-g_{\rm eq})=0\ , \tag{27}$$

$$\begin{aligned}&\frac{\partial}{\partial t}g_{ns}+(\omega_\mu\mathcal{L}_\mu+\gamma_{\mu\nu}\mathcal{L}_{\mu\nu})g_{ns}\\ &+\sum_l\tau_l^{-1}g^{(l)}_{\mu_1\mu_2\cdots\mu_l}(r)\phi_{\mu_1\mu_2\cdots\mu_l}(\hat{\mathbf{r}})=-\gamma_{\mu\nu}\mathcal{L}_{\mu\nu}g_s\ .\end{aligned} \tag{28}$$

The term involving the operator $\omega_\mu\mathcal{L}_\mu$ can be calculated from Eqs. (2.23), (2.52), and (3.7) of Ref. 9. That operator couples only tensors of the same rank $l$. We have derived a similar expression for the term containing the operator $\gamma_{\mu\nu}\mathcal{L}_{\mu\nu}$, which couples tensors of rank $l$ to those of ranks $l+2$ and $l-2$. The net result is that Eqs. (27) and (28) can be rewritten in a general form

$$\begin{aligned}&\frac{\partial}{\partial t}g^{(l)}_{\mu_1\mu_2\cdots\mu_l}+\overline{l(\boldsymbol{\omega}\times g^{(l)})}_{\mu_1\mu_2\cdots\mu_l}+\frac{2l}{2l+3}\left[r\frac{d}{dr}+\frac{3}{2}\right]\overline{\gamma_{\mu_1\lambda}g^{(l)}_{\lambda\mu_2\mu_3\cdots\mu_l}}+\tau_l^{-1}g^{l}_{\mu_1\mu_2\cdots\mu_l}\\ &=-\left[\frac{l(l-1)}{(2l-1)(2l+1)}\right]^{1/2}\left[r\frac{d}{dr}-l+2\right]\overline{\gamma_{\mu_1\mu_2}g^{(l-2)}_{\mu_3\mu_4\cdots\mu_l}}-\left[\frac{(l+2)(l+1)}{(2l+5)(2l+3)}\right]^{1/2}\left[r\frac{d}{dr}+l+3\right]\gamma_{\lambda\kappa}g^{(l+2)}_{\lambda\kappa\mu_1\mu_2\cdots\mu_l}\ .\end{aligned} \tag{29}$$

The cross product on the left-hand side of Eq. (29) stands for $\epsilon_{\mu_1\lambda\kappa}\omega_\lambda g^{(l)}_{\kappa\mu_2\mu_3\cdots\mu_l}$, where $\epsilon_{\mu\lambda\kappa}$ is the totally antisymmetric isotropic tensor of rank 3. Equation (29) leads to the following equations for the scalar, second-rank tensor ($l=2$), and fourth-rank tensor ($l=4$) contributions:

$$\frac{\partial}{\partial t}g_s+\tau_0^{-1}(g_s-g_{\rm eq})=-\left[\frac{2}{15}\right]^{1/2}\left[r\frac{d}{dr}+3\right]\gamma_{\lambda\kappa}g^{(2)}_{\lambda\kappa}\ , \tag{30}$$

$$\frac{\partial}{\partial t}g^{(2)}_{\mu\nu}+2\overline{(\omega\times g^{(2)})}_{\mu\nu}+\frac{4}{7}\left[r\frac{d}{dr}+\frac{3}{2}\right]\overline{\gamma_{\mu\lambda}g^{(2)}_{\lambda\nu}}+\tau_2^{-1}g^{(2)}_{\mu\nu}=-\left[\frac{2}{15}\right]^{1/2}\gamma_{\mu\nu}r\frac{d}{dr}g_s(r)-\frac{2}{\sqrt{21}}\left[r\frac{d}{dr}+5\right]\gamma_{\lambda\kappa}g^{(4)}_{\mu\nu\lambda\kappa}\ , \tag{31}$$

and

$$\frac{\partial}{\partial t}g^{(4)}_{\mu\nu\lambda\kappa}+4\overline{(\omega\times g^{(4)})}_{\mu\nu\lambda\kappa}+\frac{8}{11}\left[r\frac{d}{dr}+\frac{3}{2}\right]\overline{\gamma_{\mu\alpha}g^{(4)}_{\alpha\nu\lambda\kappa}}+\tau_4^{-1}g^{(4)}_{\mu\nu\lambda\kappa}$$
$$=-\frac{2}{\sqrt{21}}\left[r\frac{d}{dr}-2\right]\overline{\gamma_{\mu\nu}g^{(2)}_{\lambda\kappa}}-\left[\frac{30}{143}\right]^{1/2}\left[r\frac{d}{dr}+7\right]\gamma_{\alpha\beta}g^{(6)}_{\alpha\beta\mu\nu\lambda\kappa}\ . \tag{32}$$

Clearly the equations are the first of a hierarchy of coupled equations. Here we decouple the equations by disregarding tensors of ranks $l\geq 6$.

### B. Stokes-Maxwell relations for Couette flow

We can infer the Couette-flow Stokes-Maxwell relations for $g^{(l)}_k$ from Eqs. (30)–(32) by setting the time derivatives equal to zero and using the Couette-flow modified expressions for $g^{(2)}$ and $g^{(4)}$ given in the Appendix. To the lowest nonvanishing order in the shear rate we get to zeroth order:

$$g_s=g_{\rm eq}\ , \tag{33}$$

i.e., the equilibrium limit. To first order,

$$g^{(2)}_2=-\tau_2\gamma r\frac{d}{dr}g_s\ . \tag{34}$$

To second order,

$$\delta g_s=g_s-g_{\rm eq}(r)=-\tfrac{1}{15}\gamma\tau_0\left[r\frac{d}{dr}+3\right]g^{(2)}_2\ , \tag{35}$$

$$g^{(2)}_1=\gamma\tau_2 g^{(2)}_2\ , \tag{36}$$

$$g^{(2)}_0=\tfrac{1}{7}\gamma\tau_2\left[r\frac{d}{dr}+\frac{3}{2}\right]g^{(2)}_2\ , \tag{37}$$

$$g^{(4)}_0=-\tfrac{1}{8}\gamma\tau_4\left[r\frac{d}{dr}-2\right]g^{(2)}_2\ , \tag{38}$$

$$g^{(4)}_3=\tfrac{1}{2}\gamma\tau_4\left[r\frac{d}{dr}-2\right]g^{(2)}_2\ . \tag{39}$$

To third order,

$$g^{(4)}_2=-\gamma\tau_4\left[r\frac{d}{dr}-2\right]g^{(2)}_0+\tfrac{24}{77}\gamma\tau_4\left[r\frac{d}{dr}+\frac{3}{2}\right]g^{(4)}_0$$
$$-\tfrac{2}{11}\gamma\tau_4\left[r\frac{d}{dr}+\frac{3}{2}\right]g^{(4)}_3\ , \tag{40}$$

$$g^{(4)}_4=-2\gamma\tau_4 g^{(4)}_3-\tfrac{1}{2}\gamma\tau_4\left[r\frac{d}{dr}-2\right]g^{(2)}_1\ . \tag{41}$$

To fourth order,

$$g^{(4)}_1=\gamma\tau_4 g^{(4)}_2+\tfrac{2}{11}\gamma\tau_4\left[r\frac{d}{dr}+\frac{3}{2}\right]g^{(4)}_4\ . \tag{42}$$

We have also derived Eqs. (33)–(42) by an alternate method that is more tedious but requires less of the for-

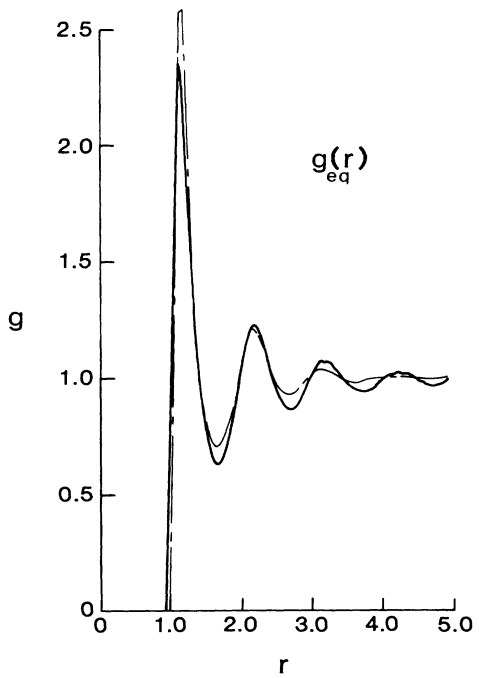


FIG. 6. The equilibrium distribution function $g_{\rm eq}(r)$ at $\rho=0.7$, solid curve, and the value calculated via Eq. (35) from the results with $\gamma=1.0$ (dashed curve).

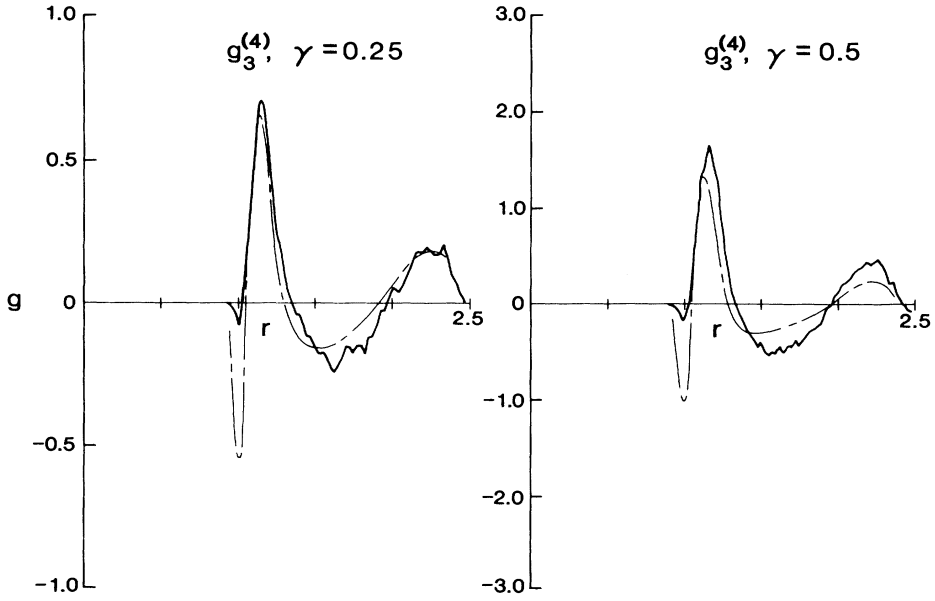


FIG. 7. The curves for $g_3^{(4)}$ for the soft-sphere system at $\rho=0.7$ and $\gamma=0.5$ and 0.25; the dashed curves are predicted from the generalized Stokes-Maxwell relations.

malism of Cartesian tensor analysis. The flow term of Eq. (19) is written as $\gamma y\, d/dx$. Upon insertion of Eqs. (13)–(15) into Eq. (19), the differential operator mixes the coefficients of $X_k^{(l)}$ and leads to a hierarchy of coupled equations. This hierarchy is solved iteratively to leading order in $\gamma\tau$, and after considerable algebra Eqs. (33)–(42) are recovered.

One should point out that Eq. (36) and the first terms in the right-hand side of Eqs. (41) and (42) arise from the term involving the vorticity in Eq. (20) so they would vanish in a vortex-free flow, e.g., Eq. (12) with $\alpha=1$. All other contributions arise from the shear-rate tensor $\gamma_{\mu\nu}$. Also, to leading order in $\gamma\tau$, only the first terms on the right-hand side of Eqs. (31) and (32) are required. The truncation of the hierarchy represented by Eqs. (30)–(32) at $l=4$ is justified to leading order in $\gamma\tau$; inclusion of the terms of rank $l\geq 6$ would affect only higher-order terms in a $\gamma\tau$ expansion.

Equations (34)–(37) were presented and tested in Ref. 10. The expression in Ref. 13 for the "cubic" fourth-rank function, which is a linear combination of $g_0^{(4)}$ and $g_3^{(4)}$, follows from Eqs. (38) and (39).

### C. Test of the relations

To test the relations, given the simulated values of $g_k^{(l)}$, we made a very simple assumption that turned out to be generally upheld, namely, that $\tau_0=\tau_2=\tau_4$. Further, rather than treat each relation in any detail we decided to determine $\tau$ *solely by comparing* the relationship of Eq. (34) with the simulated data for $g_2^{(2)}$. In fact we did this very simply by setting $\tau$ so that the minimum in the simulated and theoretical curves at small $r$ corresponded for a given value of $\gamma$. The results for $\gamma=1$ are shown in Figs. 1 and 2 as dashed curves with $\tau=0.169$. Figure 6 shows the plot for $g_{\rm eq}$. Figure 7 gives representative plots for the comparison at lower shear rates, $\gamma=0.5$ and 0.25. We show only the curves for $g_3^{(4)}$; the others follow the same trend as seen in Figs. 1, 2, and 7 and for these shear rates we found $\tau\,(\gamma=0.5)\approx 0.1$ and $\tau\,(\gamma=0.25)\approx 0.18$.

We consider the comparison between the Stokes-Maxwell expressions and the simulation data to be very good overall, with the agreement less satisfactory for the $\delta g$, $g_1^{(2)}$, and $g_0^{(4)}$ terms. Note that these last two relationships, paradoxically, are the simplest. There also does not seem to be any clear correlation between the agreement and the "order" of the expression.

## V. CONCLUSIONS

In this work we have extended our previous studies on a fluid's microstructure under shear as represented by the behavior of the pair correlation function $g(\mathbf{r},\gamma)$. Specifically we have expanded $g(\mathbf{r},\gamma)$ in terms of spherical harmonics, or Cartesian tensors, to tensor rank 4 and evaluated the coefficients by NEMD for a soft-sphere liquid. We have found that the influence of the rank 4 coefficients is not necessarily small for the soft-sphere system studied; in particular the coefficient $g_3^{(4)}$ that represents cubic symmetry is significant. The intensity plots in Fig. 5 illustrate this. As a rule of thumb, we expect the expansion for $g(\mathbf{r},\gamma)$ to reach essentially its convergent limit at $l=4$ if the condition $\tau\gamma\lesssim 0.05$ is realized. For the specific case of interest, $\tau\gamma\approx 0.2$, the expansion through $l=4$ is probably close to its limit although higher-order terms may give small but noticeable contributions.

From a general kinetic equation, Eq. (19), we have derived expressions for the coefficients of the $g(\mathbf{r},\gamma)$ expansion for Couette flow using a relaxation-time approximation, Eq. (26). If we select a single relaxation time for the system, we can predict all $g_k^{(l)}$ surprisingly well given $g_2^{(2)}$.

For example, comparing the simulated $g_2^{(2)}$ with the Stokes-Maxwell expression Eq. (34) we set $\tau=0.169$ for the system at $\rho=0.7$ and $\gamma=1.0$ and obtain the results shown in Figs. 1 and 2. But it must be stressed that the relaxation assumption is too simple and a more general theory should take into account the $\gamma$ dependence of $\tau$.

Furthermore the relaxation-time approach here must give an analytic $\gamma$ dependence for the properties of the system. This is not in agreement with the results of the computer simulations that indicate, for example,[4] that pressure varies with $\gamma^{3/2}$ and the viscosity with $\gamma^{1/2}$. Nevertheless, one has a theory that predicts the shear-induced behavior of the radial distribution function of a simple liquid, and consequently the shear-dependent macroscopic behavior, given the equilibrium radial distribution function and a relaxation time.


## ACKNOWLEDGMENTS

The authors thank D. G. Friend for valuable suggestions. The work was supported by the U.S. Department of Energy (Office of Basic Energy Sciences).


## APPENDIX: ANSATZ FOR THE EXPANSION TENSORS OF RANKS 2 AND 4

In plane Couette symmetry the tensors $g_{\mu\nu}^{(2)}$ and $g_{\mu\nu\lambda\kappa}^{(4)}$ occurring in Eq. (4) can be written as

$$\xi_2 g_{\mu\nu}^{(2)} = g_2^{(2)}\overline{e_\mu^x e_\nu^y} + g_1^{(2)}\tfrac{1}{2}(e_\mu^x e_\nu^x - e_\mu^y e_\nu^y) + g_0^{(2)}\overline{e_\mu^z e_\nu^z}\ , \tag{A1}$$

$$\xi_4 g_{\mu\nu\lambda\kappa}^{(4)} = g_0^{(4)}\overline{e_\mu^z e_\nu^z e_\lambda^z e_\kappa^z} + g_1^{(4)}\tfrac{1}{2}(\overline{e_\mu^x e_\nu^x e_\lambda^z e_\kappa^z} - \overline{e_\mu^y e_\nu^y e_\lambda^z e_\kappa^z}) + g_2^{(4)}\overline{e_\mu^x e_\nu^y e_\lambda^z e_\kappa^z}$$
$$+ g_3^{(4)}(\overline{e_\mu^x e_\nu^x e_\lambda^x e_\kappa^x} + \overline{e_\mu^y e_\nu^y e_\lambda^y e_\kappa^y} - \tfrac{3}{4}\overline{e_\mu^z e_\nu^z e_\lambda^z e_\kappa^z}) + g_4^{(4)}(\overline{e_\mu^x e_\nu^x e_\lambda^x e_\kappa^y} - \overline{e_\mu^x e_\nu^y e_\lambda^y e_\kappa^y})\ , \tag{A2}$$

where $\mathbf{e}^x, \mathbf{e}^y, \mathbf{e}^z$ are unit vectors parallel to the coordinate axis; the overbar indicates the symmetric traceless part of a tensor. The factors $\xi_2$ and $\xi_4$ are defined by Eq. (8); $\xi_2=\sqrt{15/2}$ and $\xi_4=\sqrt{315/8}$. Note that all tensors on the right-hand side of Eqs. (A1) and (A2) obey the Couette symmetry.

Insertion of (A1) and (A2) into Eq. (4) for $l=2$ and $l=4$ leads to Eqs. (13)–(15). The numerical factors occurring are somewhat arbitrary since we could multiply $X_k^{(l)}$ by a constant and compensate by dividing $C_k^{(l)}$ by the same constant; those for the second-rank tensorial functions have been chosen such that $g_2^{(2)}$, $g_1^{(2)}$, and $g_0^{(2)}$ are consistent with our previous work.[8,10–11] The functions $X_0^{(4)}$ and $X_3^{(4)}$ of (15) which follow from (A2) are linear combinations of the cubic harmonics[22] $K_{41}$ and $K_{42}$. All other functions occurring in (14) and (15) are proportional to the standard cubic harmonics,[22] which, in turn, are linear combinations of spherical harmonics.


[1]See, for example, D. J. Evans and G. P. Morriss, Comput. Phys. Rep. **1**, 299 (1984); D. J. Evans and W. G. Hoover, Annu. Rev. Fluid Mech. **18**, 243 (1986).

[2]See, for example, the special issues devoted to nonlinear fluid behavior of Physica **118A**, Nos. 1–3 (1983), edited by H. J. M. Hanley, and Physics Today **37** (1) (1984), edited by H. J. M. Hanley. See also J. R. Dorfman and T. R. Kirkpatrick, in *Proceedings of the Enrico Fermi School on Molecular Dynamics of Statistical Mechanical Systems,* edited by G. Ciccotti and W. G. Hoover (North-Holland, New York, 1986), p. 260; J. W. Dufty, J. J. Brey, and A. Santos, *ibid.*, p. 294; H. J. M. Hanley, *ibid.*, p. 317.

[3]H. J. M. Hanley, J. C. Rainwater, N. A. Clark, and B. J. Ackerson, J. Chem. Phys. **79**, 4448 (1983).

[4]J. C. Rainwater, H. J. M. Hanley, T. Paszkiewicz, and Z. Petru, J. Chem. Phys. **83**, 339 (1985); J. C. Rainwater and H. J. M. Hanley, Int. J. Thermophys. **6**, 595 (1985).

[5]H. J. M. Hanley (unpublished).

[6]K. D. Romig and H. J. M. Hanley, Int. J. Thermophys. **7**, 877 (1986).

[7]D. J. Evans and R. O. Watts, Chem. Phys. **48**, 321 (1980); W. T. Ashurst and W. G. Hoover, Phys. Rev. A **11**, 658 (1975).

[8]S. Hess and H. J. M. Hanley, Phys. Rev. A **25**, 1801 (1982).

[9]S. Hess and W. Kohler, *Formeln zur Tensor-Rechnung* (Palm & Enke, Erlangen, 1980).

[10]S. Hess and H. J. M. Hanley, Phys. Lett. **98 A**, 35 (1983).

[11]S. Hess and H. J. M. Hanley, Int. J. Thermophys. **4**, 97 (1983).

[12]For example, D. M. Heyes, J. Chem. Phys. **85**, 997 (1986); J. J. Erpenbeck, Phys. Rev. Lett. **52**, 1333 (1984); S. Hess, Int. J. Thermophys. **6**, 657 (1985); J. Mec. Theor. Appl., special issue, p. 1 (1985); D. J. Evans and G. P. Morriss, Phys. Rev. Lett. **56**, 2172 (1986).

[13]S. Hess, J. Phys. (Paris) Colloq. **46**, C3-191 (1985).

[14]S. Hess, Phys. Rev. A **22**, 2844 (1980); Physica **127 A**, 509 (1984).

[15]We have slightly changed the notation of our previous work, e.g., Refs. 10 and 11, in that we use $g_k^{(2)}$ with $k=0$, 1, and 2 in place of $k=0$, $-$, and $+$, respectively.

[16]As usual, all units are reduced with the mass, energy, and length parameters set equal to unity.

[17]D. J. Evans, H. J. M. Hanley, and S. Hess, Phys. Today **37** (1), 26 (1984).

[18]S. Hess, Physica **118 A**, 79 (1983).

[19]H. S. Green, *Structure of Liquids,* Vol. 10 of *Handbuch der Physik,* edited by S. Fluegge (Springer, Berlin, 1960).

[20]J. Schwarzl and S. Hess, Phys. Rev. A **33**, 4277 (1986).

[21]An alternate, diffusionlike form for $\mathcal{D}$ was considered by J. C. Rainwater and S. Hess, Physica **118 A**, 371 (1983).

[22]V. D. Lage and H. A. Bethe, Phys. Rev. **71**, 612 (1947); A. Hüller and J. W. Cane, J. Chem. Phys. **61**, 3599 (1974).

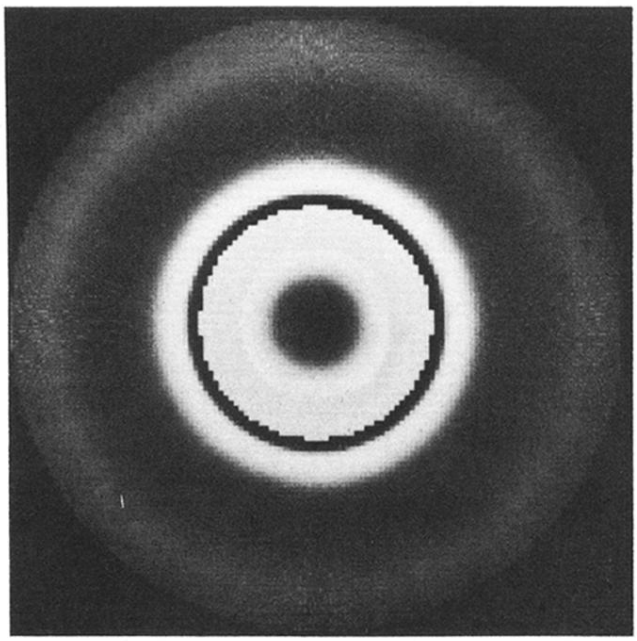

FIG. 3. Intensity plot of the scalar contribution to the distribution of particles around a central particle for the soft-sphere system at $\rho=0.7$, $\gamma=1$. The inner (darkest) ring of maximum intensity corresponds to the peak in $g_s(r)$. The center dark spot is an artifact to depict the central particle.

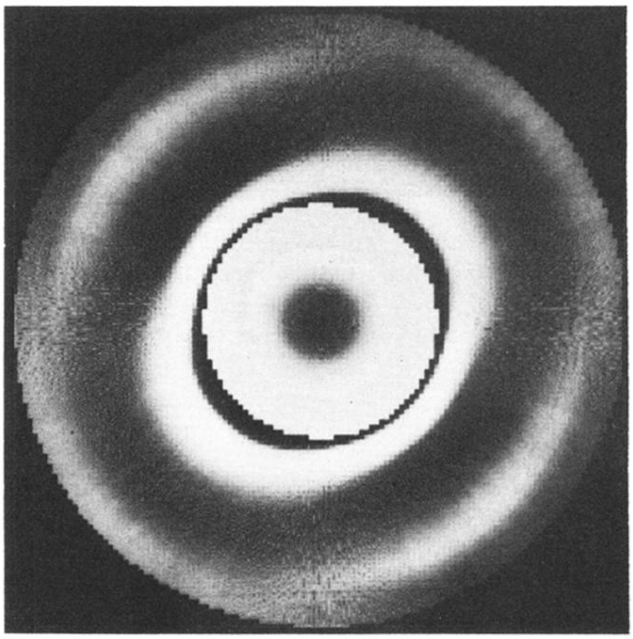

FIG. 4. Intensity plot for the soft-sphere system subjected to a shear with $\gamma = 1.0$. The plot is for the plane of the shear, see Eq. (18), with all $g_k^{(2)}$ included. The major axis of the ellipse is slightly away from $\pi/4$ and there is some weak structure in the second ring.

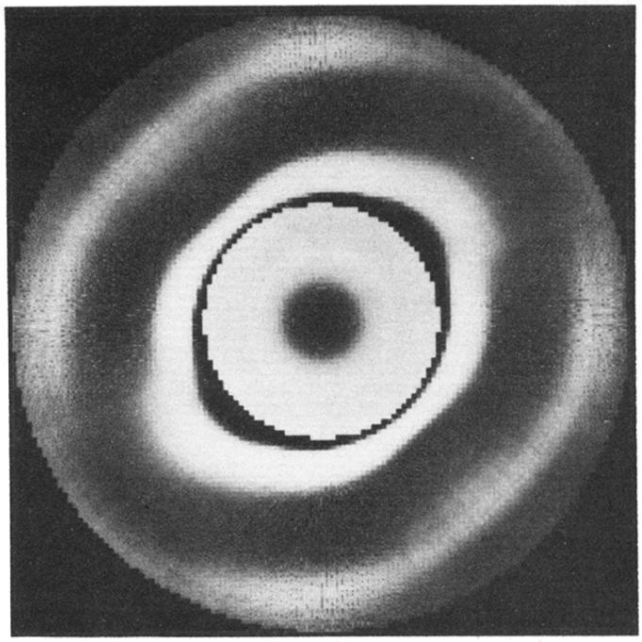

FIG. 5. In this plot all expansion coefficients of Eq. (18) are included. Note the structure changes in the second ring.